Deep crustal melt plumbing of Bárðarbunga volcano, Iceland

T. S. Hudson[1,2], R. S. White[1], A. Brisbourne[2], T. Greenfield[1†], T. Ágústsdóttir[1], and R. G. Green[1]

[1]Bullard Laboratories, Department of Earth Sciences, University of Cambridge, Cambridge, UK

[2]British Antarctic Survey, Natural Environment Research Council, Cambridge, UK

Corresponding author: T.S. Hudson (tsh37@cam.ac.uk)

† Now at: School of Ocean and Earth Sciences, University of Southampton, Southampton, SO14 3ZH, UK

Key Points:

- Microearthquakes occur in a narrow vertical zone extending from 7 to 22 km depth near Bárðarbunga volcano, Iceland
- Seismicity is inferred to be caused by melt movement with opening crack mechanisms in the mid-crust
- Earthquakes originate outside the volcano caldera, suggesting multiple melt feeders through the crust

Abstract

Understanding magmatic plumbing within the Earth's crust is important for understanding volcanic systems and improving eruption forecasting. We discuss magma plumbing under Bárðarbunga volcano, Iceland, over a four-year period encompassing the largest Icelandic eruption in 230 years. Microseismicity extends through the usually ductile region of the Earth's crust, from 7-22 km depth in a sub-vertical column. Moment tensor solutions for an example earthquake exhibits opening tensile crack behavior. This is consistent with the deep (> 7 km) seismicity being caused by the movement of melt in the normally aseismic crust. The seismically inferred melt path from the mantle source is offset laterally from the center of the Bárðarbunga caldera by ~12 km, rather than lying directly beneath it. It is likely that an aseismic melt feed also exists directly beneath the caldera and is aseismic due to elevated temperatures and pervasive partial melt under the caldera.

1 Introduction

We use microseismicity to investigate melt movement within the usually ductile region of the Icelandic crust (> 6-8 km bsl [*Key et al.*, 2011]) beneath one of Iceland's most active volcanoes, Bárðarbunga, over a four-year period including the 2014-2015 Bárðarbunga-Holuhraun eruption. Although brittle failure seismicity has been attributed to melt movement at similar depths elsewhere in the Earth's crust [*Wright and Klein*, 2006; *Key et al.*, 2011; *Shelly and Hill*, 2011; *White et al.*, 2011; *Tarasewicz et al.*, 2012; *Power et al.*, 2013; *Greenfield and White*, 2015; *Klügel et al.*, 2015; *Kiser et al.*, 2016], observations of seismicity associated with deep (> 7 km) crustal melt movement both preceding and following a volcanic eruption have until now proved elusive.

For this study, we define deep crustal melt movement as molten rock propagating within the usually ductile region of the Earth's crust. The brittle-ductile boundary varies in depth geographically, but lies ~7 km below sea level (bsl) in this region of Iceland (Figure 1). Brittle failure of the ductile crust does not occur under normal geological strain rates, so the ductile region is usually aseismic. However, if the rock is subjected to sufficiently high strain rates it can sustain brittle failure, emitting seismic energy that can be detected at the surface as a microearthquake. Melt driven by increased magmatic pressure can provide locally high strain rates sufficient to promote brittle failure [*Shelly and Hill*, 2011; *White et al.*, 2011; *Greenfield and White*, 2015]. Therefore, brittle failure microseismicity observed in the normally ductile region of the Icelandic crust can be attributed to melt movement.

2 Data

A dense seismic network operated by the University of Cambridge surrounds Bárðarbunga central volcano. Our earthquake catalogue covers 1st January 2012 to 1st August 2016, approximately two years prior to and following the 2014-2015 Holuhraun eruption. On 16th-29th August 2014, melt was fed through a 48 km long lateral dike from Bárðarbunga volcano to Holuhraun, where a six-month-long fissure eruption started on 29th August 2014 [*Sigmundsson et al.*, 2015; *Ágústsdóttir et al.*, 2016]. During the eruption, 72 three-component Cambridge seismometers were in operation, in addition to 14 instruments maintained by the Icelandic Meteorological Office (IMO) (Supplementary Figure S1). This provides good azimuthal coverage of the region surrounding Bárðarbunga, allowing calculation of well constrained locations and moment tensor solutions. The nearest long-term seismometer is VONK

(Figure 1). To improve constraints on earthquake hypocenters, two additional instruments were deployed for ~50 days from mid-June 2016, within 5 km of observed deep seismicity epicenters. This improved our understanding of how well depth is constrained with and without a station present directly above the activity. Shifts of ~2 km are observed, which is of similar magnitude to the average depth uncertainty of all manually refined events, ±2 km.

An earthquake catalogue was created by automatically detecting and locating events using the Coalescence Microseismic Mapping (CMM) technique [*Drew et al.*, 2013], then manually refining CMM derived arrival times of P and S phases of all events with initial automatic locations deeper than 7 km bsl. Single event locations were calculated using NonLinLoc [*Lomax and Virieux*, 2000] with the equal differential time method [*Font et al.*, 2004], then refined using double-difference relocation [*Waldhauser and Ellsworth*, 2000] where possible. Double-difference relocations are generally within uncertainty (Supplementary Figure S5). A velocity model based on refraction profiles [*Pálmason*, 1971; *Gebrande et al.*, 1980; *Darbyshire et al.*, 1998], with a constant V_p/V_s ratio of 1.78 [*Ágústsdóttir et al.*, 2016] was used initially for all event locations, before varying the V_p/V_s ratio to minimize the root-mean-square (rms) of the time residuals for the manually refined events only (Supplementary Figure S2). The motivation for this is that the V_p/V_s ratio in the crust below the brittle-ductile transition is otherwise poorly constrained. The final velocity model uses a V_p/V_s ratio of 1.8 (Supplementary Table 1), similar to that found beneath Askja volcano, ~50 km NE of Bardarbunga on the same rift zone [*Greenfield et al.* 2016].

3 Results

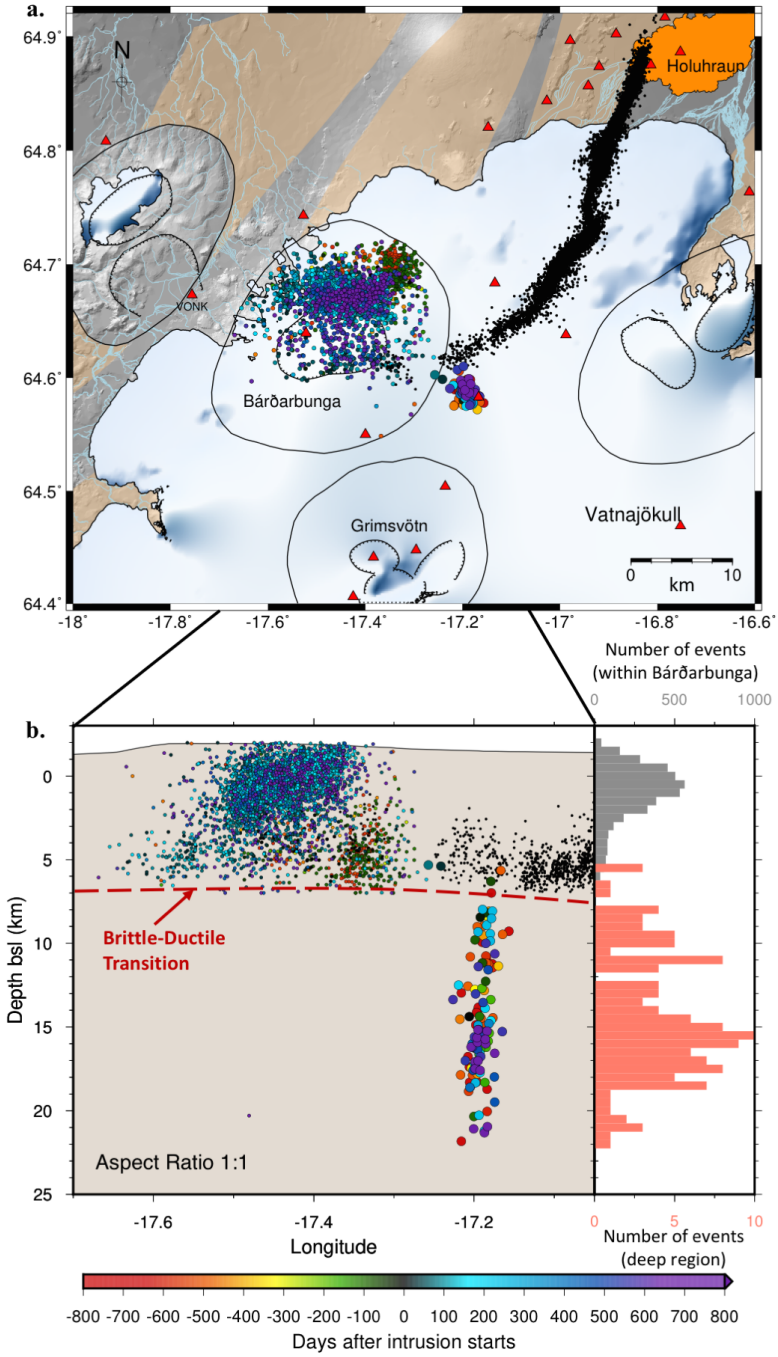

Figure 1. (a) Map showing seismicity (colored by time after start of the 2014-2015 Bárðarbunga-Holuhraun dike intrusion) from 1st January 2012 to 1st August 2016, with intrusive period seismicity (16th-29th August 2014) in black. Sand colored areas outline fissure swarms, transecting the central volcanoes (outlined by circles) of each volcanic system [*Einarsson and Saemundsson*, 1987]. Red triangles show seismic stations. (b) East-west vertical plane projection, showing seismicity in (a). All events from depths > 7 km are manually refined, with shallower seismicity plotted from 1st January 2013 to 1st August 2016. Histograms are for hypocenters within Bárðarbunga (grey), and manually refined events (red).

3.1 Shallow seismicity

Shallow seismicity (Figure 1) delineates the brittle-ductile transition at ~6-7 km depth. During the dike propagation and eruptive periods there is increased shallow activity along the path of the dike at 6-8 km depth [*Ágústsdóttir et al.*, 2016], as well as within the caldera. Of the shallow activity within Bárðarbunga volcano (< 7 km bsl), ~11 % of the ~4500 events occur before the dike intrusion started and ~89 % after (Figure 1). Seismicity on the flank of Bárðarbunga, to the immediate north-east of the caldera preceding the eruption is thought to be caused primarily by geothermal activity, while the majority of the seismic activity within and immediately north of the caldera after the intrusion is associated with caldera collapse [*Gudmundsson et al.*, 2016].

3.2 Deep seismicity

The well-defined cluster of deep seismicity (> 7 km bsl) (Figure 1), on the outer flank of the central volcano, is laterally offset by ~12 km to the south-east of the center of the Bárðarbunga caldera. The deep activity occurs primarily over depths of 10 to 22 km bsl, with no apparent temporal evolution in the depth of events (Supplementary Movie S1). A small number of events above the deep activity occur within the shallow brittle crust, at 5-7 km bsl. Manually located events have P and/or S arrival time picks on up to 40 seismometers (average of 18), with overall rms misfit uncertainties of ~ 0.1 s. We detect two to three times more deep crustal earthquakes using automatic locations than are plotted in Figure 1, within the same area of crust as those plotted. These are evident as arrivals on the closer seismometers, but we have not included them here because they are recorded on fewer stations and therefore have poorly-constrained hypocentral locations.

The daily rate of deep manually refined earthquakes (Figure 2) shows sporadic swarms, with a maximum of 4 events per day that are of sufficient amplitude to be manually refined. There appears to be an approximately constant average rate of deep seismicity over the time period, with no obvious change associated with the eruption. An apparent lack of deep seismicity during the dike intrusion and eruptive periods shown on Figure 2 could indicate a genuine lack of any melt movement at depth during that period, but it is more likely that the seismometer network is less sensitive due to the many earthquakes generated during the dike intrusion and eruption. Approximately 50,000 shallow events were detected and located in this region during the eruption [*Ágústsdóttir et al.*, 2016], thus making it harder to detect low magnitude deep events.

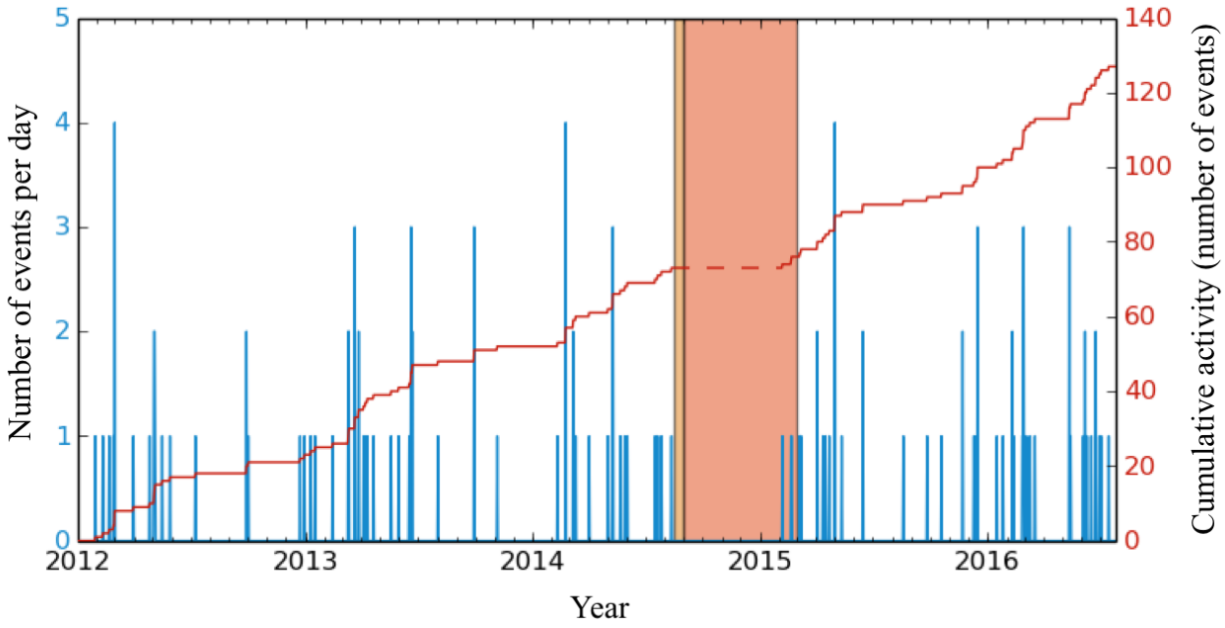

Figure 2 – Daily seismicity rate at depths of 7 to 25 km bsl, from 1st January 2012 to 1st August 2016. All hypocenters are manually refined. Light and dark orange shaded regions indicate dike propagation and eruptive periods, respectively. Red line shows cumulative number of events.

3.3 Earthquake failure mechanisms

Moment tensor inversions reveal that these deep events show non-double-couple mechanisms and have a significant opening crack component (Figure S4). We focus on one particular representative event (01:28, 15th June 2015), discussed in detail here (Figure 3). The single event location uncertainty associated with this event is plotted in Figure 3a as a scatter cloud representing the posterior probability density function, and is approximately ±1 km vertically and ±250 m horizontally. The waveforms arriving at one seismometer (VONK) are shown in Figure 3b. The earthquake has impulsive P and S phase arrivals, in common with all the events presented here. S phases have higher amplitudes than P phases, as is true for the majority of deep events. The spectrum for the event at the closest instrument has a peak in the P arrival at ~3.6 Hz and in the SH arrival at ~2.0 Hz.

Results from a full moment tensor inversion using both P and SH phase polarities are shown in a Lune plot [*Tape and Tape*, 2012] in Figure 3c, using a Bayesian method, MTFIT [*Pugh et al.*, 2016]. This provides a better constrained solution than using only P phase polarities. The most likely full moment tensor focal mechanism (Figure 3d,e) show that the example event has a component of opening tensile crack behavior. A volumetric component to the solution is required rather than a pure double couple solution (which would lie in the center of the Lune plot at the point marked 'DC').

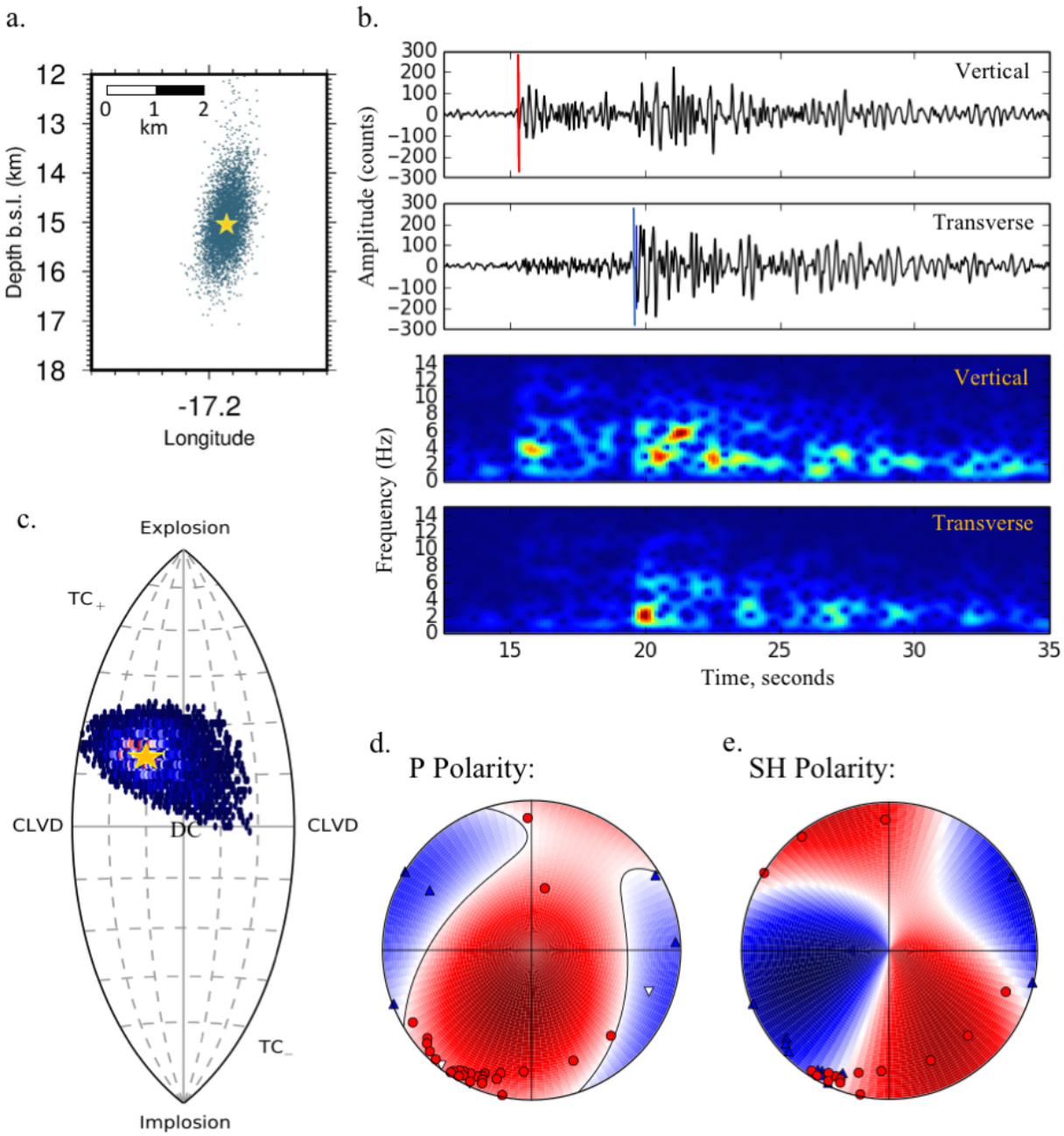

Figure 3 – Example earthquake (15th June 2015, 01:28). (a) Most probable location (gold star) and scatter representing the PDF of location uncertainty. (b) Vertical and transverse components, with associated spectrograms, recorded at station VONK (see Figure 1a for location). (c) Lune plot shows the most likely solution from the moment tensor inversion (gold star) and the associated PDF. Double-couple (DC), opening and closing tensile cracks (TC_+, TC_-) and compensated linear vector dipole (CLVD) solution locations are labeled. (d), (e) Full moment tensor solution using P and SH phase arrival polarities (phase arrivals shown in Supplementary Figure S3, with phase and station information in Tables S3 and S4). Red and blue signify compressional and dilatational arrivals, respectively.

4 Discussion

4.1 Melt induced brittle failure

The earthquake shown in Figure 3 is most likely caused by melt induced brittle failure with a volumetric component, accommodated through an opening tensile crack. At these depths in the crust a possible mechanism for this is the movement of melt at sufficient pressure to induce brittle failure of the rock, with the fluid intruded into the resulting crack providing the inferred positive volumetric increase. This is consistent with melt moving from one sill to another, shallower sill, along pathways that are opened by the melt movement. As the earthquake occurs within the normally ductile region of the Earth's crust, the fluid must be forced through the rock sufficiently fast to cause brittle failure. Similar behavior has been observed in deep seismicity under Askja volcano, ~50 km to the north-east of Bárðarbunga [*Greenfield and White*, 2015], where earthquakes caused by melt moving between crustal sills result in multiple but short-lived swarms of microseismicity. Another, less likely but still plausible, mechanism could be fracture within the melt itself. Peaks in the spectra of the earthquake at low frequencies further suggest the presence of fluid during fracture.

It is likely that the melt movement is driven by overpressures due to melt buoyancy or by high pore pressures generated by exsolution of CO_2. Seismicity triggered by transient fluid pressure increases due to CO_2 exsolved from melt are observed elsewhere [e.g. *Shelly et al.*, 2015]. There are two possible mechanisms for CO_2 exsolution driven overpressure. Firstly, CO_2 is likely to start exsolving from primitive mantle melts at depths of ~20 km as melt rises through the crust and decompresses. This mechanism could therefore trigger deep melt movement and is consistent with the main onset of deep events being at ~20 km. Alternatively, exsolution of CO_2 could occur as melt crystallizes *in situ* in a sill.

4.2 Melt propagation at depth

Bárðarbunga is one of several large subglacial volcanoes above the center of the Iceland hotspot [*Einarsson et al.*, 1997]. A clear indicator of melt accumulation at Bárðarbunga is the enhanced seismicity observed for several years prior to the 2014 Holuhraun eruption [*Brandsdóttir and Pálsson*, 2014]. Continued elevated seismicity also occurs following the eruption, potentially suggesting continued melt accumulation [*Jónsdóttir et al.*, 2017]. Melt must therefore travel up from its source in the underlying convecting mantle plume [*White and McKenzie*, 1989] through a plumbing system in order to feed Bárðarbunga volcano. Figure 4 presents a summary schematic interpretation of the melt plumbing at Bárðarbunga superimposed on our observed seismic hypocenters.

Three main factors control the deep magma plumbing in this region. First, the melt is generated at depths > 40 km, in the core of the underlying mantle plume, which has a diameter of ~100 km [*White and McKenzie*, 1989]. The initial feed of melt into the lower crust is likely to be dominated by convection and decompression melting in the mantle plume, with little influence from the volcanic edifices at the surface. There are likely to be multiple, transient feeder points into the overlying crust, of which we image just a currently active one. Second, the region under Vatnajökull is an extensional environment, although the precise location and interaction of extensional rifts under the ice cap is unknown. Nevertheless, an extensional regime, controlled by tectonic stress gradients of the divergent rift zone, could provide favorable conditions to

encourage melt to rise vertically through the crust [*Dahm*, 2000]. Third, the volcanic edifices themselves are likely to exert some control on the melt path near the surface as it is affected by the topographic loads of the volcanoes, and the influence of magma chambers [*Acocella and Neri*, 2003; *Karlstrom et al.*, 2009]. Throughout the crust, melt plumbing is likely to comprise a complex network of lateral sills, with magma rising within high density intrusive complexes near the surface (which characterize large central volcanoes in Iceland [*Pálmason*, 1971; *Brandsdóttir et al.*, 1997]).

The deep seismicity, and hence melt plumbing, observed here occurs primarily at depths of 10-20 km (Figure 4, label 1 and Supplementary Movie S1). There could be multiple reasons for the lack of seismicity below 22 km, even though melt must travel up from below this depth. It may be that the energy emitted by fracture at these depths is highly attenuated, and so not recorded well at the surface; or that the crust is hotter and more ductile at greater depths, requiring higher strain rates for fracture with insufficient fluid pressures to drive this; or that there is no sill formation, which may be required for the pressure of melt to build; or perhaps melt might instead ascend aseismically via buoyant diapirs at these depths [*Rubin*, 1993]. An absence of sill formation at depths below 20-25 km could be caused by insufficient rigidity contrasts, or by insufficient melt temperature and flow rates that control the formation of sills when solidification of melt is considered [*Kavanagh et al.*, 2006; *Chanceaux and Menand*, 2014].

One intriguing observation is that the spread of seismicity with depth is relatively continuous, within the depth uncertainty, likely indicating a continuous, linked vertical conduit. Elsewhere along the northern volcanic rift of Iceland, there are multiple pockets of seismicity caused by melt within the deep crust [e.g. *Key et al., 2011*; *Greenfield and White*, 2015]. However, these are isolated pockets of activity that are interpreted as sills, unlike the vertical melt conduit extending through the crust that we image here.

Although deep seismic activity is confined to the SE outer flank of Bárðarbunga, this lateral offset is not an unusual observation [*White and McCausland*, 2016]. Other volcanoes such as Askja (Iceland) [*Greenfield and White*, 2015], Kilauea (Hawaii) [*Wright and Klein*, 2006; *Bell and Kilburn*, 2012; *Wech and Thelen*, 2015; *Lin and Okubo*, 2016], Mount St Helens (US) [*Kiser et al.*, 2016] and El Hierro (Canary Islands) [*Klügel et al.*, 2015] also have deep seismicity with similar lateral offsets from the associated volcanoes.

In some other volcanoes, there is evidence of laterally offset melt plumbing that leads to magma bypassing the main caldera melt source, indicated by petrological constraints. For example, in Krafla lavas erupted to the north of the caldera during the 1975-84 eruptions exhibit marked petrological and geochemical differences from those lavas erupted within the caldera, suggesting that they bypassed the magma reservoir under the caldera [*Gronvold et al.*, 2008]. Likewise, in the hotspot volcano of Kilauea, primitive compositions show that magma may bypass the summit storage region on its way to the eruption site [*Vinet and Higgins*, 2010]. Our seismic results may capture an instance of some melt bypassing the main caldera storage region.

4.3 Interactions of deep melt plumbing with shallow volcanic systems

Sparse seismicity is also observed in the shallow, brittle crust at ~ 5-7 km bsl, above the column of deep seismicity (Figure 1). There was no other seismicity in the shallow crust east of

the Bárðarbunga caldera in the period prior to the August 2014 dike injection (during and after which there was abundant seismicity along the dike path), so we assume that this is related to the underlying deep column of seismicity. It is possible that it is due to volatile release from the deeper melt triggering pre-stressed rupture in the brittle crust, as has been interpreted above the Upptyppingar melt injection to the north [*White et al.,* 2011]. However, we interpret this pre-dike shallow seismicity as indicating that at least a small volume of melt traveled up to the brittle crust at ~6 km bsl (Figure 4, label 2) because several of the events are offset laterally towards the eventual location of the dike, as would be expected for small volumes of melt moving laterally near the base of the brittle crust.

A speculative interpretation is that these small amounts of melt in the upper crust may have influenced the dike propagation from Bárðarbunga in August 2014. This is near the location where the dike turned a 90° corner, from traveling southeast to northeast, on 16th August 2014 (64.6°N, -17.26°E, Figure 4a), approximately along strike of the local rift zone. At this corner, even the initial dike tip propagation occurred aseismically over a 4 km distance (Figure 4a, label 2, and Supplementary Movie S1) and this section of the dike remained aseismic throughout the eruption while melt passed through it. This contrasts with the intense seismicity along the rest of the dike path as the tip of the dike cracked its way forward (Figure 4, label 3). However, as soon as the dike had propagated toward the northeast the subsequent melt flow through it was aseismic [*Ágústsdóttir et al.,* 2016]. Therefore, the lack of seismicity as the dike propagated through this aseismic corner (Figure 4, label 2) prompts the interpretation that at least a small amount of melt, or elevated temperatures caused by melt fed through the deep column we map, was present in this region prior to the dike propagation, and may also provide a reason for the abrupt change in direction of propagation of the dike at this location.

It is perhaps surprising that if the deep earthquakes are caused by melt moving upwards, they are not also found directly beneath the Bárðarbunga caldera. However, this may be a consequence of the relatively short period of observation of seismicity, since there are also no deep seismically active feeders currently present under the other nearby hotspot volcanoes of Kverkfjöll and Grímsvötn. Or, perhaps most likely, if the entire crust directly under the caldera is hotter with pervasive pockets of melt, then melt may move through it aseismically. The seismic velocity of the upper crust under the hotspot volcanoes has markedly lower surface wave velocities than elsewhere in Iceland (0.5 km s^{-1} slower), indicating the presence of pervasive melt or elevated temperatures [*Green et al.*, 2017]. The deep column of seismicity we observe may only represent relatively minor melt movement through cooler crust outside the caldera. The presence of seismicity gives no indication of the volume of melt that may flow through this deep sub-vertical feeder.

The abrupt decrease in seismicity at 6-7 km depth bsl under Bárðarbunga caldera provides an uppermost depth bound on the main melt storage region (Figure 4, label 4). We have not found any seismicity under Bárðarbunga caldera > 7 km bsl (except for one single event at 19 km depth after the eruption), providing a strong constraint on the likely upper limit of the melt storage region. However, the shallow Bárðarbunga reservoir must have contained a significant volume of melt in order to feed the 1.9 ± 0.3 km^3 Holuhraun intrusion and eruption [*Gudmundsson et al.*, 2016]. The primary melt storage region under Bárðarbunga is therefore likely to be shallower than the ~10.5-11 km bsl depth assumed by *Gudmundsson et al.* [2016].

We believe that a shallower melt storage region still satisfies the geodetic, deformation and petrologic constraints presented by *Gudmundsson et al.* [2016]. Geodetic modeling based on

InSAR and GPS data constrains a Mogi pressure deflation source under the caldera to depths of ~6-10 km bsl (8-12 km below surface) [*Gudmundsson et al.*, 2016]. *Gudmundsson et al*. [2016] suggest that the melt source lies at the bottom of this range, whereas our inferred melt source lies at the top of this range, so both models are consistent with the deformation. Their choice of a deeper melt deflation source is based primarily on geobarometry, which indicates melt residence at pressures of 3.5-5.5 kbar (12-19 km depth below surface using an average crustal density of 2800 kg/m3). Recent work by *Hartley et al.* [2017] indicates that the most probable melt inclusion equilibration pressures lie between 2.5 to 4.2 kbar (corresponding to depths of 9 - 15 km below surface), with the carrier melt equilibrating at 2.1+/-0.7 kbar, c. 7.5 km depth below surface (6 km bsl). These geobarometry estimates are less precise than the seismicity control on depth, but are consistent with our model of the main melt reservoir equilibrating at a depth of 6-7 km bsl, with crystals mixed in from underlying sills at greater depths up to 13 km bsl. These observations are also consistent with those at the nearby volcano Askja, where melt imaged by seismic tomography lies at a similar depth of 6 km bsl, with multiple deeper sills under the volcano extending down to 20 km depth [*Greenfield et al.* 2016]. The adjacent hotspot volcano of Grimsvötn has a melt region with its upper surface at an even shallower depth of ~ 3 km bsl [*Alfaro et al.*, 2007], whilst the Krafla magma chamber is similar with its top at ~ 3 km bsl [*Brandsdóttir et al.*, 1997].

The major remaining question with our model is how melt might feed this shallow melt storage region under Bárðarbunga volcano. It is probable that it simply rises vertically from the underlying mantle aseismically, through a series of staging sills under the caldera (Figure 4b). When solidified, the stack of intrusive sills would produce the relatively high-velocity core reported from beneath the Krafla caldera [*Brandsdóttir et al.*, 1997], with a magma chamber sitting at the top. However, if the column of seismicity southeast of the caldera is the only, or main melt feed route from the mantle, then the melt would have to migrate laterally along a sill at a depth of ~10 km bsl. This corresponds to the top of the most intense column of seismicity, and a peak in inferred depths from geobarometry, so it remains a possibility. However, since there is no seismicity or other direct evidence for this putative sill, we believe that such a route for melt feeding the shallow Bárðarbunga storage region is unlikely.

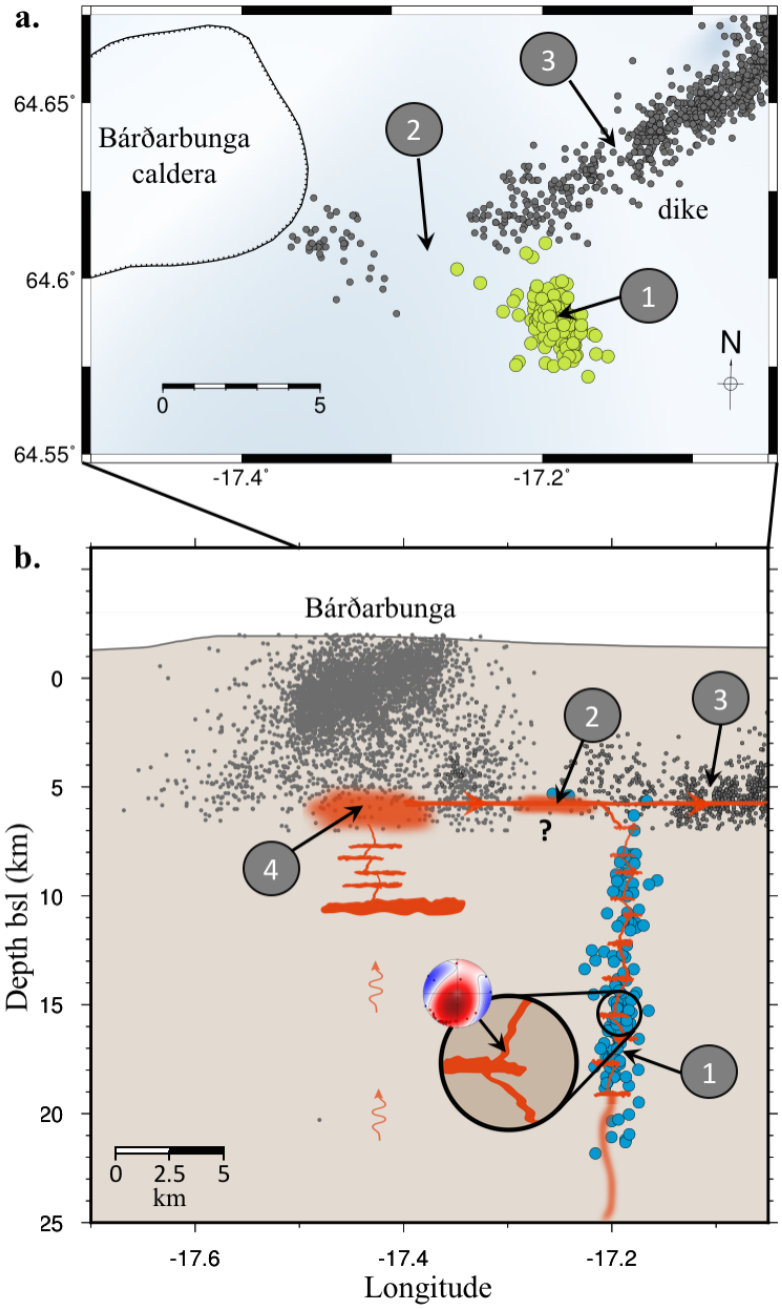

Label	Brief Description
1	Deep seismicity indicating melt plumbing
2	Possible shallow melt storage region in aseismic dike gap
3	Seismicity associated with dike intrusion
4	Main shallow Bárðarbunga melt storage region

Figure 4 – Interpretation of melt plumbing under Bárðarbunga volcanic system, superimposed on recorded seismicity. (a) map view with dike events; (b) Seismicity projected onto an east-west cross-section with no vertical exaggeration. Blue and green dots show hypocenters with manual arrival phase picks. Regions of melt (orange shading) are inferred from seismicity, geodesy and geochemistry [*Green et al.*, 2015; *Sigmundsson et al.*, 2015; *Ágústsdóttir et al.*, 2016; *Gudmundsson et al.*, 2016]. See text for discussion of numbered labels and Supplementary Movie S1 for time sequence animation.

5 Conclusions

Persistent seismicity extending through the crust from 7-22 km depth bsl is observed before and after an eruption of Bárðarbunga to the southeast of the caldera and is little affected by the eruption itself. The seismicity is interpreted as caused by melt movement. The deep seismicity is laterally offset from the center of Bárðarbunga's caldera by ~12 km, indicating that melt can travel from depth at significant distances from the near-surface volcanic system. Similar deep seismic activity laterally offset from the shallow volcanic system is observed at many other volcanoes. Furthermore, it suggests that there may be multiple seismic and aseismic feeders for the melt rising through the crust beneath active volcanoes. It is therefore important to monitor deep melt movement that feeds volcanoes at distances up to 20 km or more from the main caldera, in order to understand better when a volcano might be receiving melt from depth and hence more likely to erupt.

Acknowledgments and Data

Seismometers were borrowed from the Natural Environment Research Council (NERC) SEIS-UK (loans 968 and 1022), and the NERC British Antarctic Survey. Funding was by research grants from the NERC and the European Community's Seventh Framework Program Grant No. 308377 (Project FUTUREVOLC), and a number of graduate studentships from the NERC. We thank Sveinbjörn Steinthórsson, Heidi Soosalu, Ágúst Þór Gunnlaugsson, Magnús Tumi Gudmundsson, Finnur Pálsson, the Icelandic Glaciological Society and many others who have assisted with fieldwork in Iceland. We thank Jonathon Smith for contributions to the supplementary information. Margaret Hartley kindly provided details of her geochemical analyses of Holuhraun lavas in advance of publication. The Icelandic Meteorological Office, Chris Bean (Dublin Institute for Advanced Studies) and the British Geological Survey kindly provided additional data from seismometers in north-east Iceland; data delivery from IMO seismic database 20151001/01. Hypocenter locations of deep events are listed in Table S2, along with phase information for each event (Table S3) and station locations (Table S4). Seismic waveform data is deposited in the SeisUK archive. We thank David Hill and an anonymous reviewer for contributions that helped improve the manuscript. Department of Earth Sciences, Cambridge contribution number ESC4000.

References

Acocella, V., and M. Neri (2003), What makes flank eruptions? The 2001 Etna eruption and its possible triggering mechanisms, *Bull. Volcanol.*, *65*(7), 517–529, doi:10.1007/s00445-003-0280-3.

Ágústsdóttir, T., J. Woods, T. Greenfield, R. G. Green, R. S. White, T. Winder, B. Brandsdóttir, S. Steinthórsson, and H. Soosalu (2016), Strike-slip faulting during the 2014 Bárðarbunga-Holuhraun dike intrusion, central Iceland, *Geophys. Res. Lett.*, *43*(4), 1495–1503, doi:10.1002/2015GL067423.

Alfaro, R., B. Brandsdóttir, D. P. Rowlands, R. S. White, and M. T. Gudmundsson (2007), Structure of the Grímsvötn central volcano under the Vatnajökull icecap, Iceland, *Geophys. J. Int.*, *168*(2), 863–876, doi:10.1111/j.1365-246X.2006.03238.x.

Bell, A. F., and C. R. J. Kilburn (2012), Precursors to dyke-fed eruptions at basaltic volcanoes: insights from patterns of volcano-tectonic seismicity at Kilauea volcano, Hawaii, *Bull. Volcanol.*, *74*(2), 325–339,

doi:10.1007/s00445-011-0519-3.
Brandsdóttir, B., and F. Pálsson (2014), Unrest within Bárðarbunga and Grímsvötn 1838-1903, *Jökull*, *64*, 91–106.
Brandsdóttir, B., W. Menke, P. Einarsson, R. S. White, and R. K. Staples (1997), Faroe-Iceland Ridge Experiment 2. Crustal structure of the Krafla central volcano, *J. Geophys. Res.*, *102*(96), 7867–7886.
Chanceaux, L., and T. Menand (2014), Solidification effects on sill formation: an experimental approach, *Earth Planet. Sci. Lett.*, *403*, 79–88, doi:10.1016/j.epsl.2014.06.018.
Dahm, T. (2000), Numerical simulations of the propagation path and the arrest of fluid-filled fracture in the Earth, *Geophys. J. Int.*, *141*, 623–638.
Darbyshire, F. A., I. T. Bjarnason, R. S. White, and Ó. G. Flóvenz (1998), Crustal structure above the Iceland mantle plume imaged by the ICEMELT refraction profile, *Geophys. J. Int.*, *135*(3), 1131–1149, doi:10.1046/j.1365-246X.1998.00701.x.
Drew, J., R. S. White, F. Tilmann, and J. Tarasewicz (2013), Coalescence microseismic mapping, *Geophys. J. Int.*, *195*(3), 1773–1785, doi:10.1093/gji/ggt331.
Einarsson, P., and K. Saemundsson (1987), *Earthquake Epicenters 1982-1985 and Volcanic Systems in Iceland: Upptok Jardskjalfta 1982-1985 Og Eldstodvakerfi a Islandi*, Menningarsjodur.
Einarsson, P., B. Brandsdóttir, M. T. Gudmundsson, H. Björnsson, K. Grínvold, and F. Sigmundsson (1997), Center of the Iceland hotspot experiences volcanic unrest, *Eos, Trans. Am. Geophys. Union*, *78*(35), 369–375, doi:10.1029/97EO00237.
Font, Y., H. Kao, S. Lallemand, C. S. Liu, and L. Y. Chiao (2004), Hypocentre determination offshore of eastern Taiwan using the maximum intersection method, *Geophys. J. Int.*, *158*(2), 655–675, doi:10.1111/j.1365-246X.2004.02317.x.
Gebrande, H., H. Miller, and P. Einarsson (1980), Seismic structure of Iceland along RRISP profile I, *J. Geophys. Fur Geophys.*, *47*(1–3), 239–249.
Green, R. G., T. Greenfield, and R. S. White (2015), Triggered earthquakes suppressed by an evolving stress shadow from a propagating dyke, *Nat. Geosci. Lett.*, *8*, doi:10.1038/NGEO2491.
Green, R. G., K. F. Priestley, and R. S. White (2017), Ambient noise tomography reveals upper crustal structure of Icelandic rifts, *Earth Planet. Sci. Lett.*, *466*, 20–31, doi:10.1016/j.epsl.2017.02.039.
Greenfield, T., and R. S. White (2015), Building Icelandic igneous crust by repeated melt injections, *J. Geophys. Res. Solid Earth*, *120*(11), 7771–7788, doi:10.1002/2015JB012009.
Gronvold, K., S. A. Halldorsson, G. Sugurdsson, G. Sverrisdottir, and N. Oskarsson (2008), Isotopic systematics of magma movement in the Krafla central volcano, north Iceland, in *Geochimica et Cosmochimica Acta Supplement, Goldschmidt Conference Abstracts*, vol. 72, p. 331.
Gudmundsson, M. T. et al. (2016), Gradual caldera collapse at Bárdarbunga volcano, Iceland, regulated by lateral magma outflow, *Science*, *353*(6296), 262, doi:10.1126/science.aaf8988.sciencemag.org.
Hartley, M. E., E. Bali, S. A. Halldórsson, J. Maclennan, D. A. Neave, and D. W. Peate (2017), Holuhraun 2014-2015: Geochemical constraints on magma storage and transport during a major volcano- tectonic episode, *Jt. Assem. TSG-VMSG-BGA, Liverpool*, 108. Available from: https://www.liverpool.ac.uk/media/livacuk/tsg-vmsg-bga/documents/Joint-Assembly_web-version.pdf
Jónsdóttir, K. et al. (2017), Bárðarbunga volcano - post-eruption trends following the Holuhraun eruption in 2014-2015, *Geophys. Res. Abstr.*, *19*, 12535.
Karlstrom, L., J. Dufek, and M. Manga (2009), Organization of volcanic plumbing through magmatic lensing by magma chambers and volcanic loads, *J. Geophys. Res. Solid Earth*, *114*(10), 1–16, doi:10.1029/2009JB006339.
Kavanagh, J. L., T. Menand, and R. S. J. Sparks (2006), An experimental investigation of sill formation and propagation in layered elastic media, *Earth Planet. Sci. Lett.*, *245*(3–4), 799–813, doi:10.1016/j.epsl.2006.03.025.
Key, J., R. S. White, H. Soosalu, and S. S. Jakobsdottir (2011), Multiple melt injection along a spreading segment at Askja, Iceland, *Geophys. Res. Lett.*, *38*(5), 1–5, doi:10.1029/2010GL046264.
Kiser, E., I. Palomeras, A. Levander, C. Zelt, S. Harder, B. Schmandt, S. Hansen, K. Creager, and C. Ulberg (2016), Magma reservoirs from the upper crust to the Moho inferred from high-resolution Vp and Vs models beneath Mount St. Helens, Washington State, USA, *Geology*, *44*(6), 1–4, doi:10.1130/G37591.1.
Klügel, A., M.-A. Longpré, L. García-Cañada, and J. Stix (2015), Deep intrusions, lateral magma transport and related uplift at ocean island volcanoes, *Earth Planet. Sci. Lett.*, *431*, 140–149, doi:10.1016/j.epsl.2015.09.031.
Lin, G., and P. G. Okubo (2016), A large refined catalog of earthquake relocations and focal mechanisms for the Island of Hawai'i and its seismotectonic implications, *J. Geophys. Res. Solid Earth*, *121*(7), 5031–5048,

433 doi:10.1002/2016JB013042.
434 Lomax, A., and J. Virieux (2000), Probabilistic earthquake location in 3D and layered models, *Adv. Seism. Event*
435 *Locat. Vol. 18 Ser. Mod. Approaches Geophys.*, 101–134.
436 Pálmason, G. (1971), *Crustal structure of Iceland from explosion seismology*, Prentsmidjan Leiftur.
437 Power, J. A., S. D. Stihler, B. A. Chouet, M. M. Haney, and D. M. Ketner (2013), Seismic observations of Redoubt
438 Volcano, Alaska - 1989-2010 and a conceptual model of the Redoubt magmatic system, *J. Volcanol.*
439 *Geotherm. Res.*, *259*, 31–44, doi:10.1016/j.jvolgeores.2012.09.014.
440 Pugh, D. J., R. S. White, and P. A. F. Christie (2016), A Bayesian method for microseismic source inversion,
441 *Geophys. J. Int.*, *206*(2), 1009–1038, doi:10.1093/gji/ggw186.
442 Rubin, A. M. (1993), Dikes vs. diapirs in viscoelastic rock, *Earth Planet. Sci. Lett.*, *117*(3–4), 653–670,
443 doi:10.1016/0012-821X(93)90109-M.
444 Shelly, D. R., and D. P. Hill (2011), Migrating swarms of brittle-failure earthquakes in the lower crust beneath
445 Mammoth Mountain, California, *Geophys. Res. Lett.*, *38*(20), 1–6, doi:10.1029/2011GL049336.
446 Shelly, D. R., T. Taira, S. G. Prejean, D. P. Hill, and D. S. Dreger (2015), Fluid-faulting interactions: Fracture-mesh
447 and fault-valve behavior in the February 2014 Mammoth Mountain, California, earthquake swarm, *Geophys.*
448 *Res. Lett.*, *42*(14), 5803–5812, doi:10.1002/2015GL064325.
449 Sigmundsson, F. et al. (2015), Segmented lateral dyke growth in a rifting event at Bárðarbunga volcanic system,
450 Iceland., *Nature*, *517*(7533), 191–5, doi:10.1038/nature14111.
451 Tape, W., and C. Tape (2012), A geometric setting for moment tensors, *Geophys. J. Int.*, *190*(1), 476–498,
452 doi:10.1111/j.1365-246X.2012.05491.x.
453 Tarasewicz, J., B. Brandsdottir, R. S. White, M. Hensch, and B. Thorbjarnardottir (2012), Using microearthquakes
454 to track repeated magma intrusions beneath the Eyjafjallajokull stratovolcano, Iceland, *J. Geophys. Res. Solid*
455 *Earth*, *117*(2), 1–13, doi:10.1029/2011JB008751.
456 Vinet, N., and M. D. Higgins (2010), Magma solidification processes beneath Kilauea volcano, Hawaii: A
457 quantitative textural and geochemical study of the 1969-1974 Mauna Ulu Lavas, *J. Petrol.*, *51*(6), 1297–1332,
458 doi:10.1093/petrology/egq020.
459 Waldhauser, F., and W. L. Ellsworth (2000), A double-difference earthquake location algorithm: method and
460 application to the Northern Hayward Fault, California, *Bull. Seismol. Soc. Am.*, *90*(6), 1353–1368,
461 doi:10.1785/0120000006.
462 Wech, A. G., and W. A. Thelen (2015), Linking magma transport structures at Kilauea volcano, *Geophys. Res. Lett.*,
463 *42*(17), 7090–7097, doi:10.1002/2015GL064869.
464 White, R., and W. McCausland (2016), Volcano-tectonic earthquakes: A new tool for estimating intrusive volumes
465 and forecasting eruptions, *J. Volcanol. Geotherm. Res.*, *309*, 139–155, doi:10.1016/j.jvolgeores.2015.10.020.
466 White, R., and D. McKenzie (1989), Magmatism at rift zones: The generation of volcanic continental margins and
467 flood basalts, *J. Geophys. Res.*, *94*(B6), 7685-7729, doi:10.1029/JB094iB06p07685.
468 White, R. S., J. Drew, H. R. Martens, J. Key, H. Soosalu, and S. S. Jakobsdottir (2011), Dynamics of dyke intrusion
469 in the mid-crust of Iceland, *Earth Planet. Sci. Lett.*, *304*(3–4), 300–312, doi:10.1016/j.epsl.2011.02.038.
470 Wright, T. L., and F. W. Klein (2006), Deep magma transport at Kilauea volcano, Hawaii, *Lithos*, *87*(1–2), 50–79,
471 doi:10.1016/j.lithos.2005.05.004.
472
473
474
475